





Nano and micro manure amendments decrease degree of phosphorus saturation and colloidal phosphorus release from agriculture soils

Sangar Khan^a, Chunlong Liu^b, Paul J. Milham^c, Kamel Mohamed Eltohamy^{a,d}, Yasir Hamid^a, Junwei Jin^a, Miaomiao He^e, Xinqiang Liang^{a,b}  

Show more 

 Outline |  Share  Cite

<https://doi.org/10.1016/j.scitotenv.2022.157278> 

[Get rights and content](#) 

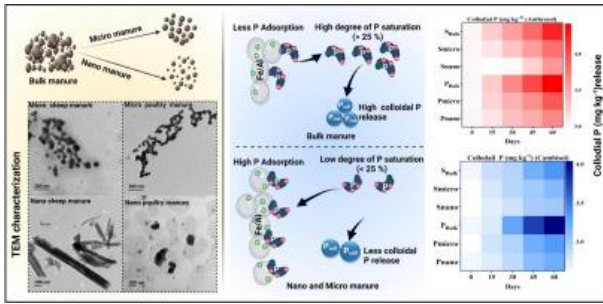
Highlights

- Nano and micro manures were rich in phosphate minerals.
- Nano manures reduced degree of phosphorous saturation and colloidal phosphorus release.
- Nano manures increased P adsorption on soils.

Abstract

The manure fertilizer increases the phosphorus (P) saturation of soils and the colloidal P release to water bodies. Manure of different particle-sizes may have different effects on colloidal P release by soil, and to date there is limited knowledge on colloidal P release from soils amended with different size manures. We produced sheep micro- (S_{Micro}) and nano-manure (S_{Nano}), and poultry micro- (P_{Micro}), nano-manure (P_{Nano}) from bulk samples by wet fractionation method. The fractionation reduced the P contents of micro- and nano-manures, and enriched them in ash and calcium, iron (Fe), magnesium, and aluminum (Al) phosphate minerals compared with the bulk manures. The degree of P saturation (DPS) in Anthorsol and Cambisol was decreased (S_{Micro} , 17.6 and 17.2 %; S_{Nano} , 14.5 and 13.3 % and P_{Micro} , 19.0 and 19.7 mg kg⁻¹; P_{Nano} , 17.0 and 14.3 mg kg⁻¹) and released less colloidal P (S_{Micro} , 3.12 and 3.78 mg kg⁻¹; S_{Nano} , 3.01 and 3.56 mg kg⁻¹ and P_{Micro} , 3.34 and 3.92 mg kg⁻¹; P_{Nano} , 3.21 and 3.65 mg kg⁻¹) than the soils receiving the bulk manures. The decrease in colloidal P was correlated with less DPS in both soils amended with micro and nano manures. That is, the only measurable effect of manure particle size on colloidal P release from the amended soils was due to chemical fractionation during separation of the size fractions. It was suggested that nano and micro manures were the effective approach to reduce colloidal P release from manure amended soils.

Graphical abstract



Download : [Download high-res image \(320KB\)](#)

Download : [Download full-size image](#)

[<](#) Previous

Next [>](#)

Keywords

Agricultural soil; Colloidal phosphorus; Manure; Nano; Phosphorus saturation

1. Introduction

Phosphorus (P) is a critical nutrient in agriculture (Xiao et al., 2020) however, excessive usage of manure-based P-fertilizers has increased ecological issues such as water eutrophication (Chen et al., 2018). The P loss from soil to water (Pan et al., 2019), whether in dissolved, colloidal, and/or particulate forms, leads to eutrophication of freshwater (Chen and Arai, 2020).

Soil colloids (1–1000 nm) possess a high surface area, resulting in a high affinity for P binding (Wang et al., 2021; Khan et al., 2021), and have essential ecological relevance (Eltohamy et al., 2021). The mineral colloids are largely Fe-/Al-/Ca-rich, although Mn oxyhydroxides and soils clay minerals may also contributed to attached P (Missong et al., 2016; Gérard, 2016). There organic colloids consist of humic acid, or natural organic matter (lipids, peptides) bind the P by making organic-mineral-P complex (Pagel et al., 2008; Sharma et al., 2017). The colloidal P release in soil depending on a variety of factors (Fresne et al., 2021), especially those related to the P sorption capacity (DPS) (Ilg et al., 2008; Li et al., 2021). However, Gottselig et al. (2014) found no correlation between colloidal Fe/Al and colloidal P concentration.

Nonetheless, manures often accelerate the release and loss of phosphorus from the manure amended soil to the aquatic system (Moradi et al., 2020), and excessive manure applications were particularly problematic (Schmieder et al., 2018). Furthermore, as per studies, the organic colloids found in manure-based fertilizer enhance the vertically movement of colloidal P (McGechan, 2002). Application of manure can also promote the colloidal P release (Liang et al., 2016), Makris et al. (2006) found 25 % increase in P loss due to colloid facilitated transport in manure amended silt loam soil. It has been investigated in soil column study that colloid particles present in manure, promote colloidal P release (Zang et al., 2013). The manure amended soils have high DPS (Khan et al., 2022), less adsorption of P (Abdala et al., 2015) which effect the colloidal P status (Fresne et al., 2021).

Although there has been a lot of study on colloidal P release in manure-amended soils, but some question still remains unanswered. There have been several studies on colloidal P release in manure amended soils (Zang et al., 2013; Eltohamy et al., 2021), including swine manure promotes the migration of colloidal P from agriculture soil, (Liang et al., 2016), poultry manure increased the degree of P saturation and colloidal P release in Cambisol and Anthrosol (Khan et al., 2022). However up to date the role of different manure components (size) on colloidal P has yet to be investigated.

We tested the hypothesis that micro and nano manure reduce the degree of P saturation and colloidal P contents in Anthrosol and Cambisol under the controlled conditions.

2. Materials and methods

2.1. Manure preparation

Air-dried sheep and poultry manure were purchased from Green Yun Fertilizer Co., Ltd., Hebei province, China. The process of manure production is shown in Fig. S1. Briefly, the manure was sieved (1 mm) and stored in plastic bags. The micro and nano manures were obtained using wet separation ([Wang et al., 2013](#)). In brief, 12.0 g of manure was stirred with 1 L of deionized water for 2 min and sonicated >20 kHz (ultrasonic power 650 W) (KQ – 500E, Kunshan ultrasonic instrument, Co. Ltd. China) for 30 min at 25 °C. The pH of the manure suspensions was accustomed to 7.0 using 0.1 mM sodium bicarbonate solution, then the suspensions were poured into 1 L cylinders for 24 h to make sure all the particles are settled down. The suspended particles (< 2 µm diameter) were separated by siphon ([Wang et al., 2013](#); [Brewer et al., 2014](#)) and labeled as sheep and poultry micro manure (S_{Micro} and P_{Micro}). For nano manure, part of the preceding suspensions was centrifuged at 3500 ×g for 30 min giving S_{Nano} and P_{Nano} manures ([Song et al., 2019](#)). The supernatant contains a size fraction <100 nm ([Zhang et al., 2013](#)). For size confirmation, the 450-nm membrane filter (Millipore, Billerica, MA, USA) was used ([Yang et al., 2019](#)). All the suspensions were freeze-dried and stored in a desiccator (over silica gel) for further use.

2.2. Manure characterization

The pH of the different size manure fractions was measured at a ratio of 1:25 (manure: water). Subsamples of freeze-dried manure (1.0 g) were processed with, reagent-grade sulfuric acid and reagent-grade hydrogen peroxide. Digests were diluted to 10 mL and analyzed for Mg, Fe, Ca, and Al by inductively coupled plasma-optical emission spectroscopy (ICP-OES) (ICAP 6000 series, Thermo Fisher Scientific, USA) ([Schwartz et al., 2011](#)). In the manure suspensions the total organic C was measured by using a dedicated analyzer (Vario MAX CNX, Elementar, Germany). The minerals in the freeze-dried manures were characterized using X-ray diffraction (Bruker D8 Advance, USA). The incident radiation was Cu K α and scattering was measured across a range of 10–80° at 2° min⁻¹. The functional groups in manures were identified by Fourier transform infrared spectroscopy (FTIR) (Model 5700 FTIR spectrophotometer, Nicolet Co., USA) at 400–4000 cm⁻¹ with a resolution of 2 cm⁻¹ using pressed potassium bromide (KBr) discs with a 1/200 mass ratio (manure/KBr). The hydrodynamic size distribution of manures in suspensions containing 200 mg of manure L⁻¹ of pure water was measured by a Zetasizer (Nano ZS90, Malvern, UK). The zeta potential of manures was measured on manure suspensions (200 mg L⁻¹) after sonication for 30 min at >20 kHz (ultrasonic power 650 W) and 30 °C (Nano ZS90, Malvern, UK). Aliquots of the same suspensions (200 mg L⁻¹), were dried onto a thin carbon-supported copper grid and the morphology was observed by an environmental transmission electronic microscope (TEM) (Model H-9500, Hitachi, Japan) ([Song et al., 2019](#)). The particle size of all six different manure fractions was measured on the evaporite from nano drops of 200 mg L⁻¹ manure suspensions on a carbon disk using scanning electron microscopy (Gemini SEM 300; ZEISS, Germany).

2.3. Soil characteristics

Surface soil (0–20 cm) of a Cambisol and an Anthrosol ([FAO, 2014](#)) was sampled from Chang Xing (119°55'34"N, 30°54'27"E) in Zhejiang province, China. Soil samples were collected from three different places by core sampler in each field, bulked, air-dried, and passed through a 2 mm sieve. Rice had been cultivated on the Anthrosol for >10 years, while Asparagus (*Asparagus Officinalis*) had been planted on the Cambisol for 7 years. In Anthrosol and Cambisol the total P (TP) was 0.32 and 0.51 g gk⁻¹, the total carbon was 3.8 and 9.0 g kg⁻¹. The Mehlich3 extracted P were 45 and 52 mg kg⁻¹, Fe were 72 and 65 mg kg⁻¹, while Al were 35 and 32 mg kg⁻¹ in the Anthrosol and Cambisol respectively. The physiochemical properties of both soils are specified in supplementary information Table S 1.

2.4. Incubation experiment

One hundred g of soil was added to twelve plastic beakers (500 mL capacity; three replicates) and sheep bulk (S_B) micro (S_{Micro}), nano (S_{Nano}) and poultry bulk (P_B), micro (P_{Micro}) and nano (P_{Nano}) manures were added at rates that supplied 11 kg of manure P ha⁻¹ to the soils at their natural bulk densities of 1.5 and 1.6 g cm⁻³, and an assumed incorporation depth of 15 cm, i.e., equal to 33 mg P kg⁻¹ of soil. The contents of the beakers were watered to ~60 % of the water holding capacity. The beakers were covered with lids that had a 10 – mm diameter hole for gas exchange. Moisture content was maintained by watering to the initial mass every third day. On days 0, 15, 30, 45, and 60 the soil

was tipped out of the beakers and sampled. The bulk soil was returned to the beakers and incubation continued. The sample (~ 50 g) was air-dried and separated into two groups: one group was crushed by hand into small aggregates and used for colloidal P and mineral analysis; and the second was crushed, sieved at 2 mm, and utilized for all later analysis.

2.5. Soil analysis

Soil pH was measured on 1:5 (m: v) suspension in water after shaking the suspension for 30 min. Total P was determined by processing the soil with sulfuric and perchloric acids in block heater set at 300 °C for 2 h. The molybdenum blue method of [Murphy and Riley \(1962\)](#) method was used for digested samples.

Colloidal P fractions (colloidal P, colloidal MRP and MUP) were determined in the initial soil samples, briefly as follows: at room temperature, the soil with small aggregates (10 g) and 80 mL of pure water were shaken (160 rpm) for 24 h. Suspensions were centrifuged for 10 min at 3000 g and then filtered by 1 m, Millipore filter paper (Billerica, MA, USA).

The initial filtrate (5 mL) were cast-off, and the rest was stored (S_I). One part of S_I was centrifuged through a < 3 kDa membrane at 4000 ×g for 45 (Millipore) and the filtrate was labeled sample B (S_{II}) ([Liang et al., 2010](#)). The filtrates S_I and S_{II} were assumed to contain colloidal and non-colloidal P, respectively. The both samples aliquots were processed in 180 mmol. L⁻¹ sulfuric acid with potassium persulfate ([Pagel et al., 2008](#)). The processed and unprocessed solutions were used for Molybdate reactive P (MRP_{coll}) determination ([Murphy and Riley, 1962](#)). The both solutions were processed with HNO₃ and H₂O₂ at 170 °C for colloidal Fe, Ca, and Al ([EPA, 2002](#)) and were determined by ICP-OES. Total organic C in both the S_I and S_{II} were analyzed by a TOC analyzer (Vario MAX CNX, Elementar, Germany) ([Niyungeko et al., 2018](#)).

The differences between S_I and S_{II} sample fractions were used to determine the concentrations of colloidal P, MRP_{coll}, colloidal total organic carbon (TOC_{coll}), colloidal minerals (Fe, Al and Ca).

The MUP_{coll} was determined as follows:

$$\text{Colloidal MUP} = \text{Colloidal P} - \text{MRP}_{\text{coll}}$$

2.6. Adsorption isotherms

P-sorption was determined batch wise conferring to [Fink et al. \(2016\)](#). Briefly, in a 50 mL centrifuge tube, soil of about 1 g was added., followed by a solution of P, as potassium dihydrogen phosphate at 0, 0.5, 1, 2, 5, 8, 10, 15, and 50 mg P L⁻¹ in 25 mL of potassium chloride (10 mmol L⁻¹) as the electrolyte. Microbial activity was inhibited by adding chloroform ([Khan et al., 2021](#)). The suspensions were centrifuged then filtered through 0.45 m filter paper after being shaken at 180 rpm for 24 h (Millipore, Billerica, MA, USA), the solids were kept for P-desorption measurement and the solution in tubes was calorimetrically tested for P ([Murphy and Riley, 1962](#)). The Langmuir isotherm was used by Origin software version 9.8 (USA) was used to estimate the concentrations of sorbed and residual P in solution by using the following equations:

$$\text{Langmuir equation } q = \frac{b \cdot Q_{\text{max}} \cdot C}{1 + bC} \quad (1)$$

In Eq. (1), q represents adsorbed P (mg kg⁻¹), Q_{max} represents maximal P adsorb (mg kg⁻¹), b represents a parameter associated with binding energy of P (L mg⁻¹), and C represents the equilibrium concentration of P. The residual soil pellets were used to assess P desorption ([Eduah et al., 2019](#)). Briefly, each centrifuge tube received 20 mL of potassium chloride solution (10 mmol L⁻¹), and agitated for 3 h at 25 °C, and centrifuged for 10 min at 3500 rpm. After three extractions, the P was determined in filtered supernatants.

The formula was used to calculate the fraction of P that was desorbed.:

$$P \text{ desorption } (\%) = \frac{\text{desorb P (mg / kg)}}{\text{adsorb P (mg / kg)}} \times 100 \quad (2)$$

2.7. Oxalate extractable P, Fe, and Al and degree of P saturation

Oxalate P (P_{ox}), Fe (Fe_{ox}), and Al (Al_{ox}) were extracted by shaking one gram of soil with 40 mL of ammonium oxalate solution at pH 3.0 for 2 h in dark ([Niyungeko et al., 2018](#)). The oxalate extracted solution were filtered (0.45 μm;

Millipore), and the P_{ox} , Fe_{ox} , and Al_{ox} were analyzed by ICP-OES. The DPS was calculated according to (Eq. (3)) (Dari et al., 2015).

$$DPS\% = \frac{P_{ox}}{(Fe_{ox} + Al_{ox})} \quad (3)$$

In Eq. (3) the P_{ox} , Fe_{ox} and Al_{ox} represent the oxalate extractable P, Fe and Al.

2.8. Statistical analysis

Data were arranged to two-way analysis of variance to estimate the effect of different manure sizes, and their interactions, on the colloidal P fractions, and minerals in both soils. Means were compared by Tukey's multiple comparison test ($p < 0.05$). Langmuir and Freundlich isotherms calculated by the Fit Adsorption Isotherm package in Origin Lab (version 2021b, USA). Correlation analysis was performed to test the significance of the pairwise relations of colloidal P with colloidal Fe, Al, and Ca.

3. Results

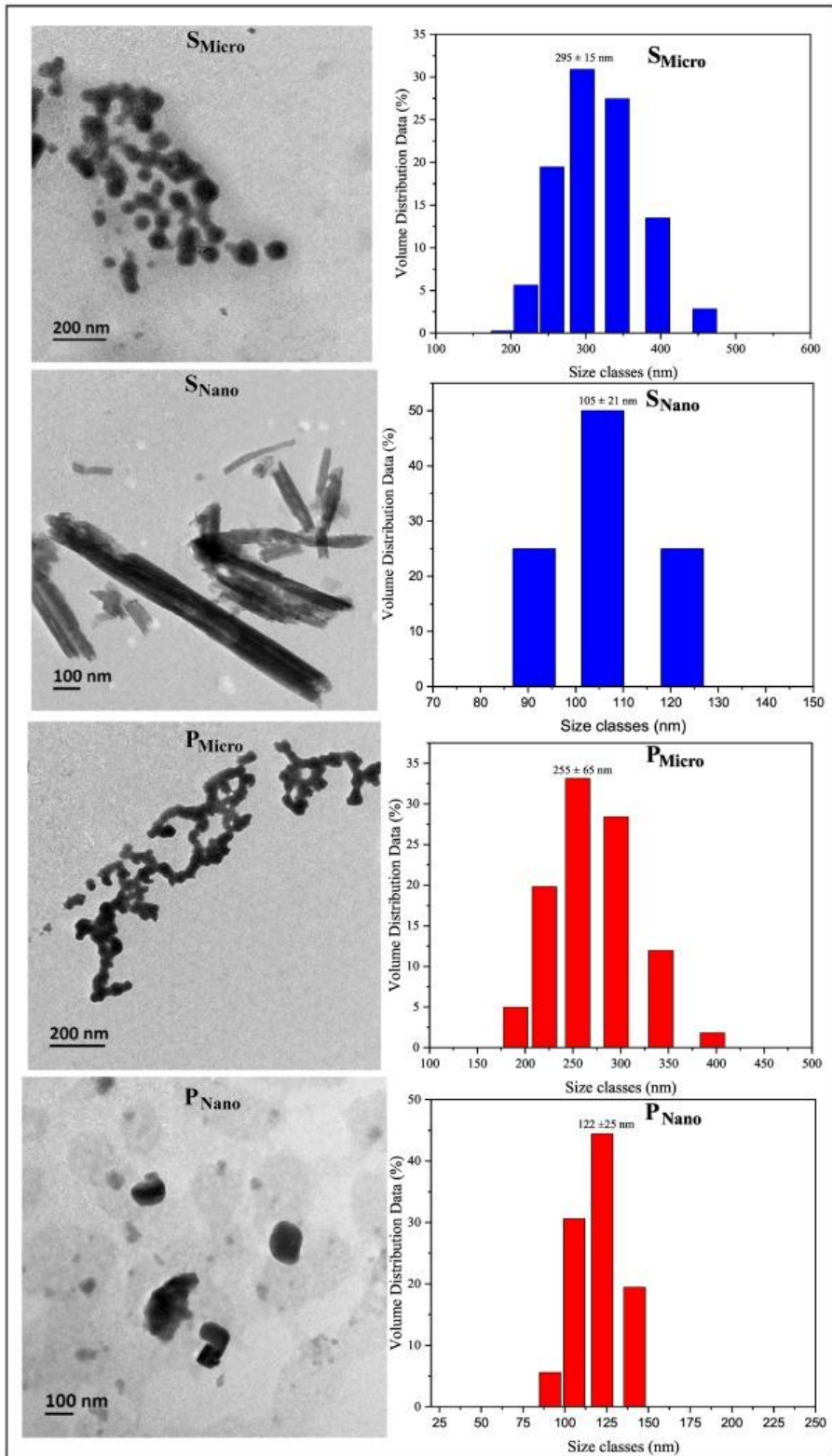
3.1. Physicochemical properties of micro and nano manures

The S_{Nano} and P_{Nano} had zeta potentials of -34.6 and -16.8 , followed by the S_{Micro} and P_{Micro} (-23.5 and -12.8), while the S_B and P_B values were (-16.6 and -13.2) (Table 1). The ash was rich in S_{Nano} and P_{Nano} , followed by S_{Micro} , P_{Micro} as compared to S_B and P_B (Table 1). The TP contents decreased and the Mg, Ca, Fe, and Al contents as the manure size decreased from bulk to smallest size (Table 1). In addition, the S_B and P_B had a greater total C contents (258 and 215 g kg^{-1}) than S_{Micro} and S_{Nano} (185 and 105 g kg^{-1}) and P_{Micro} and P_{Nano} (148 and 90.0 g kg^{-1}). The TEM showed that the shape of S_{Micro} , P_{Micro} , and P_{Nano} particles was spherical and that the S_{Nano} shape was needle-like (Fig. 1). The hydrodynamic diameter of S_{Micro} and P_{Micro} ranged between 250 and 300 nm and the S_{Nano} and P_{Nano} were smaller than 125 nm (Fig. 1). The SEM showed the particle diameter varied with the manure size fractions, i.e., it was 207 – 635 nm and 98 – 116 nm for S_{Micro} , S_{Nano} imaged at 3.0 μm and 500 nm, and 329 – 657 nm and 65.5 – 92.6 nm for P_{Micro} and P_{Nano} at 3.0 μm and 500 nm magnification scale (Fig. S2).

Table 1. Chemical and physical properties of sheep bulk (S_B), micro (S_{Micro}), nano (S_{Nano}) and poultry bulk (P_B), micro (P_{Micro}) and nano (P_{Nano}) manures.

| Types | Sheep manure | | | Poultry manure | | |
|--------------------|-------------------|--------------------|--------------------|-------------------|-------------------|-------------------|
| | S_B | S_{Micro} | S_{Nano} | P_B | P_{Micro} | P_{Nano} |
| P (g kg^{-1}) | 9.60 ± 1.55^a | 7.72 ± 2.98^b | 5.96 ± 3.85^d | 7.36 ± 2.10^b | 6.22 ± 0.51^c | 5.78 ± 0.19^d |
| C (g kg^{-1}) | 285 ± 6.85^a | 180 ± 5.45^c | 105 ± 8.25^e | 215 ± 2.91^b | 148 ± 2.51^d | 90 ± 3.12^f |
| Mg (mg kg^{-1}) | 115 ± 2.65^d | 131 ± 2.98^b | 156 ± 3.12^a | 105 ± 1.25^e | 115 ± 1.61^d | 123 ± 1.69^c |
| Ca (mg kg^{-1}) | 125 ± 1.96^c | 135 ± 1.45^b | 157 ± 2.85^a | 85 ± 2.12^f | 102 ± 2.54^e | 119 ± 4.81^d |
| Fe (mg kg^{-1}) | 131 ± 3.21^f | 141 ± 6.25^d | 161 ± 3.45^a | 121 ± 4.65^e | 148 ± 2.96^c | 151 ± 3.31^b |
| Al (mg kg^{-1}) | 121 ± 3.30^c | 135 ± 2.65^b | 155 ± 2.19^a | 112 ± 1.28^d | 125 ± 1.67^c | 150 ± 1.10^a |
| Ash contents (%) | 33 ± 1.25^d | 38 ± 1.90^c | 45 ± 1.65^a | 25 ± 0.59^e | 35 ± 0.36^d | 41 ± 0.45^b |
| Zeta potential | -29 ± 0.56^b | -23.5 ± 0.48^c | -34.5 ± 0.25^a | -13 ± 0.19^e | -12 ± 0.36^e | -16 ± 0.25^d |

Means (significance tested by LSD; $P < 0.05$) followed by SE the same letter(s) within each column are not significantly different among treatments ($p < 0.05$).



[Download : Download high-res image \(1MB\)](#)

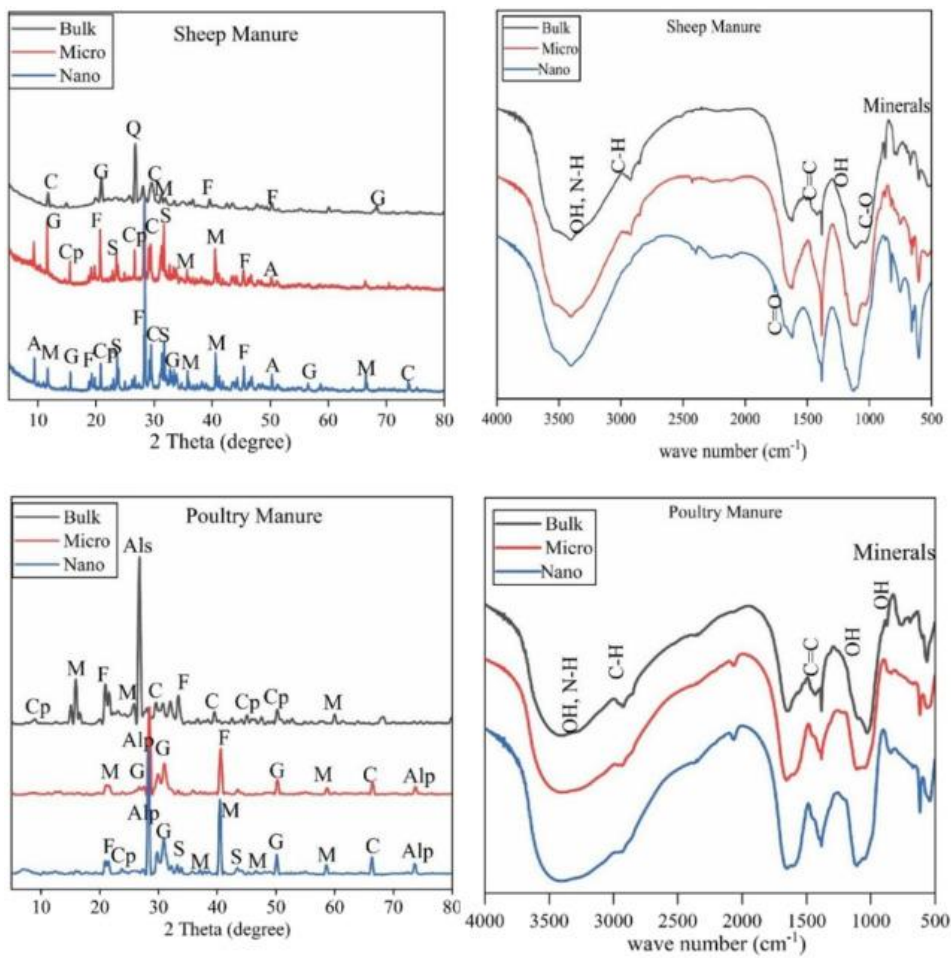
[Download : Download full-size image](#)

Fig. 1. TEM image and particle distribution of sheep micro (S_{Micro}), nano (S_{Nano}) and poultry micro (P_{Micro}), nano (P_{Nano}) manure size.

3.2. Infra-red bands and X-ray diffraction

In the infrared spectra, all manure sizes absorbed at 3500 cm^{-1} corresponding with the frequency attributed to C – OH and N – H groups. In addition, a strong peak at 1600 cm^{-1} indicated the presence of C = C in the S_{Nano} which was not observed in S_{Micro} and S_B ; similarly, the C = C group is also more abundant in P_{Nano} than in P_B and P_{Micro} (Fig. 2). The

functional group wavenumber assignments are shown in Table S2.



[Download : Download high-res image \(352KB\)](#)

[Download : Download full-size image](#)

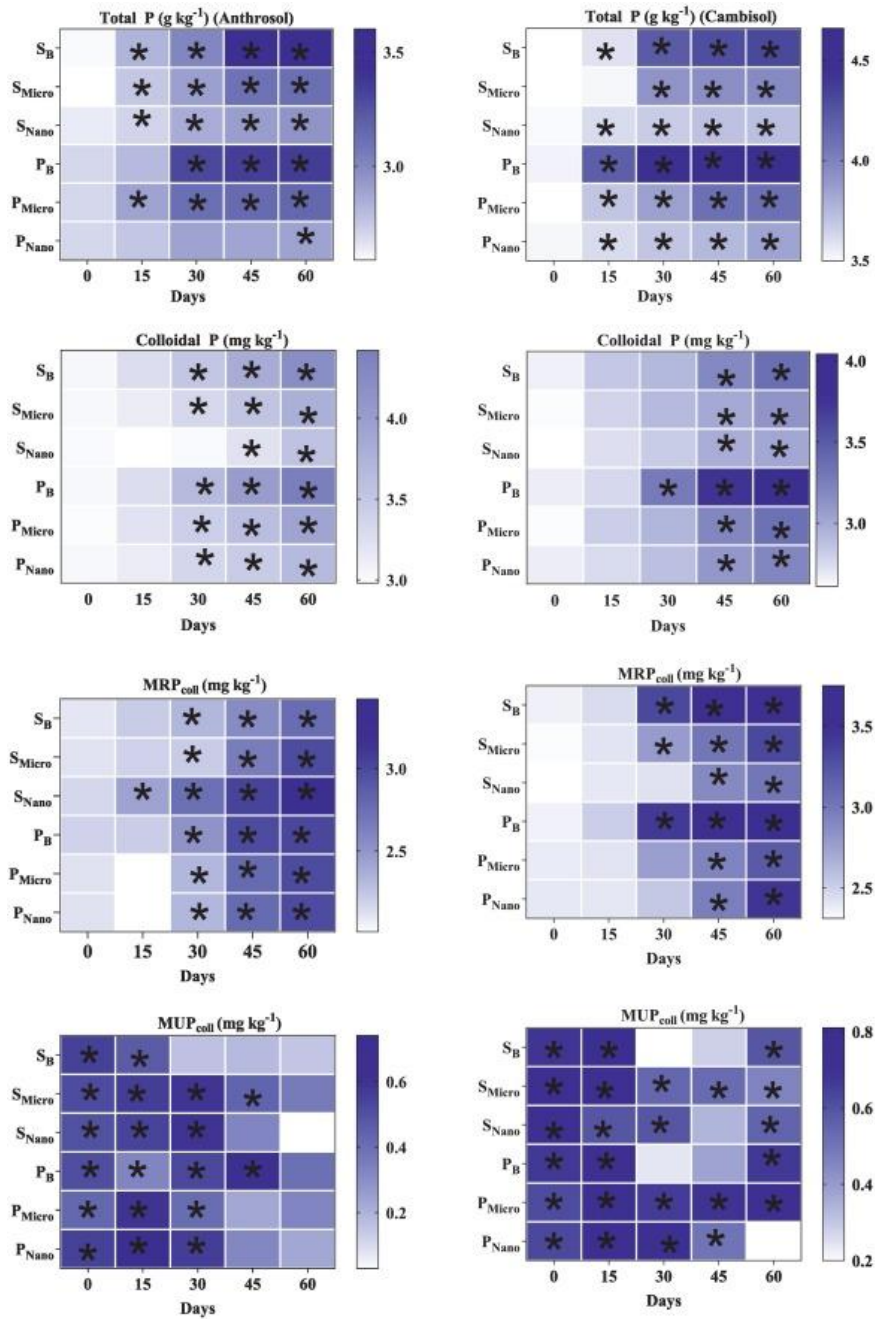
Fig. 2. XRD and FTIR spectra of Sheep and Poultry (bulk, micro and nano) manure size. In XRD, A = $\text{CaSO}_4(\text{PO}_4\text{OH})$, Alp = AlPO_4 , Als = AlSiO_3 , C = CaCO_3 , Cp = CaPO_4 , G = CaSO_4 , F = FePO_4 , M = MgPO_4 , Q = SiO_2 , S = NH_4MgPO_4 .

In x-ray diffraction, S_B exhibited strong peaks of silica (SiO_2) (28.6°), and calcium sulfate ($\text{CaSO}_4 \cdot 2\text{H}_2\text{O}$) (20.8°) (Fig. 2). In contrast, S_{Micro} and S_{Nano} lacked the SiO_2 peak but had strong peaks for $\text{CaSO}_4 \cdot 2\text{H}_2\text{O}$, and ferrous phosphate ($\text{FePO}_4 \cdot \text{H}_2\text{O}$), and peaks for magnesium phosphate ($\text{MgPO}_4 \cdot \text{H}_2\text{O}$) and struvite occurred at 23.5° and 35.2° respectively. In P_B , the strong band at 26.6° was assigned to AlSiO_3 and at 25.6° to MgPO_4 (25.6°) while the P_{Micro} and P_{Nano} did not show the presence of AlSiO_3 , but instead exhibited strong peaks of AlPO_4 (28.6°), gypsum (32°), $\text{FePO}_4 \cdot \text{H}_2\text{O}$, $\text{MgPO}_4 \cdot \text{H}_2\text{O}$ and calcium minerals (Fig. 2).

3.3. Effect of micro and nano manures on colloidal P

Application of different sizes of manure increased the TP ($P < 0.05$) in both soils. In the Anthrosol the S_B and P_B increased the TP from 2.66 to 3.36 and 2.67–4.04 g kg^{-1} , respectively (Fig. 3). The S_B and P_B increased ($P < 0.05$) the colloidal P from 2.62 to 3.39 and 2.61–4.04 mg kg^{-1} , and in the S_{Nano} and P_{Nano} treatments, the colloidal P was 2.61–2.90 and 2.67–3.21 mg kg^{-1} , respectively (Fig. 3). Similarly, in the Cambisol the S_B and P_B increased ($P < 0.05$) the colloidal P from 3.04 to 4.21 and 3.01–4.42 mg kg^{-1} respectively while with S_{Nano} and P_{Nano} treatment, the colloidal P fluctuated from 3.02 to 3.78 and 3.01–3.92 mg kg^{-1} . (Fig. 3). The MRP in Anthrosol and Cambisol increased by the addition of S_B (2.11–3.21 and 2.36–3.62 mg kg^{-1}) and P_B (2.16–3.42 and 2.35–3.75 mg kg^{-1}) (Fig. 3). The MRP in S_{Micro} and P_{Micro} ranged from 2.10 to 2.56 and 2.19–3.01 mg kg^{-1} in Anthrosol and Cambisol (2.32–3.32 and 2.38–3.21 mg kg^{-1}), respectively (Fig. 3). The addition of S_{Nano} and P_{Nano} to the Anthrosol soils increased MRP (2.11–2.98 and 2.12–2.97 mg kg^{-1}) and Cambisol (2.31–3.01 and 2.39–3.45 mg kg^{-1}). In the Anthrosol bulk sheep manure had high MUP content than the S_{Micro} and S_{Nano} , while in the case of poultry manure, P_{Nano} had the most effect on MUP

concentration followed by P_{Micro} . In Cambisol the P_B has a high content of MUP followed by S_{Micro} and S_{Nano} , and the same trend was observed in poultry manure.



[Download : Download high-res image \(829KB\)](#)

[Download : Download full-size image](#)

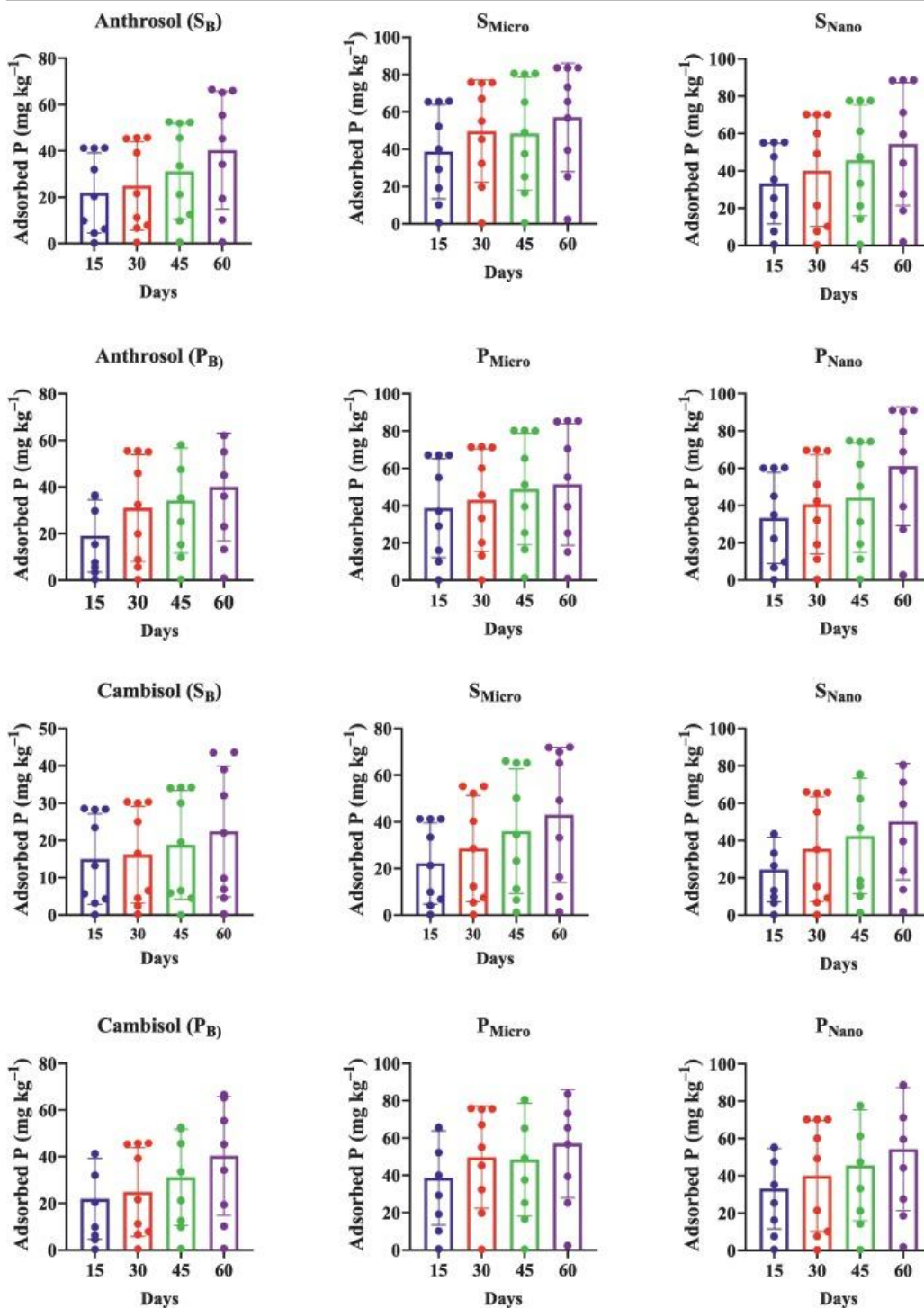
Fig. 3. Effect of sheep bulk (S_B) micro (S_{Micro}), nano (S_{Nano}) and poultry bulk (P_B), micro (P_{Micro}) and nano (P_{Nano}) manures on TP ($g\ kg^{-1}$), colloidal P ($mg\ kg^{-1}$), MRP_{coll} ($mg\ kg^{-1}$) and MUP_{coll} ($mg\ kg^{-1}$) in the Anthrosol and the Cambisol soils. The * showed that the treatments are significantly different from each other in two soils with and without *P. vittata* plantation based on LSD $p < 0.005$.

3.4. Colloidal minerals, TOC, and pH

As time progressed, the manures additions increased the concentrations of colloidal Fe, Ca, and Al and the effect was greater in both soils types the smaller the manure size. In both soil types, the pH tended to increase in the first 30 d and of incubation to gradually decrease in the following 30 days. The TOC_{coll} concentration increased in the first 45 d, then declined to the 60 d with all treatments in both soil types (Fig. S3).

3.5. P sorption, desorption, and DPS

The logarithmic form of the Langmuir isotherm described the P sorption in both soils well ($R^2 = 0.86-0.99$). After 60 d of incubation, equilibrium P sorption for the Anthrosol increased ($P < 0.05$) in the treatment order: S_{Nano} (91.2 mg kg^{-1}) $>$ P_{Nano} (88.4 mg kg^{-1}) $>$ S_{Micro} (85.3 mg kg^{-1}) $>$ P_{Micro} (83.6 mg kg^{-1}) (Fig. 4), and a similar trend was observed in the Cambisol. The Q_{max} was significantly lower than S_{B} and P_{B} in both soil types (Table S5).



[Download : Download high-res image \(1MB\)](#)

[Download : Download full-size image](#)

Fig. 4. Effect of sheep bulk (S_{B}) micro (S_{Micro}), nano (S_{Nano}) and poultry bulk (P_{B}), micro (P_{Micro}) and nano (P_{Nano}) manures on P sorption in the Anthrosol and the Cambisol soils. The dots represent the initial P concentration (0, 0.5, 1, 2, 5, 8, 10, 15, and 50 mg P L^{-1}) for P sorption isotherm.

Both soil types exhibited maximum desorption of P as follows: $S_{\text{B}} > P_{\text{B}} > S_{\text{Micro}} > P_{\text{Micro}} > S_{\text{Nano}}$ (Fig. S4). The S_{Nano} and

P_{Nano} treatments in the Anthrosol and Cambisol desorbed a smaller proportion of P (40–48 and 45–56 %) as compared to the S_{B} (57–65 %) and P_{B} (57–75 %) respectively. It was noted that the Anthrosol desorbed less P than the Cambisol across all the treatments (Fig. S4).

Amendment with S_{Nano} and P_{Nano} increased the concentrations of Fe_{ox} and Al_{ox} in both soils more than in their S_{B} and P_{B} counterparts (Table 2). In both soils, the P_{ox} concentration followed the order: $S_{\text{B}} > S_{\text{Micro}} > S_{\text{Nano}}$ and $P_{\text{B}} > P_{\text{Micro}} > P_{\text{Nano}}$, while the Fe_{ox} and Al_{ox} ordered as $S_{\text{Nano}} > S_{\text{Micro}} > S_{\text{B}}$ and $P_{\text{Nano}} > P_{\text{Micro}} > P_{\text{B}}$. In the Anthrosol the S_{B} and P_{B} had high DPS_{ox} (52.4 % and 60.9 %) at 60 days of incubation, while in the Cambisol the corresponding data were (56 % and 65 %).

Table 2. Ammonium oxalate extractable P, Al and Fe and calculated P sorption indices.

| Soil | Treatment | days | P_{ox} (mg kg ⁻¹) | Fe_{ox} (mg kg ⁻¹) | Al_{ox} (mg kg ⁻¹) | DPS_{ox} (%) | |
|--------------------|--------------------|--------------------|--|--|--|------------------------------|--------------------------|
| Anthrosol | S_{B} | 45 | 2.32 ± 0.35 ^d | 2.10 ± 0.19 ^h | 2.32 ± 0.15 ^b | 52.4 ± 1.20 ^c | |
| | | 60 | 2.54 ± 0.21 ^b | 2.71 ± 0.01 ^e | 2.91 ± 0.52 ^e | 45.2 ± 2.12 ^d | |
| | S_{Micro} | 45 | 1.07 ± 0.25 ^g | 3.20 ± 0.29 ^d | 2.70 ± 0.20 ^g | 18.1 ± 1.56 ^f | |
| | | 60 | 1.21 ± 0.11 ^e | 3.61 ± 0.31 ^b | 3.20 ± 0.46 ^c | 17.6 ± 1.54 ^f | |
| | S_{Nano} | 45 | 1.00 ± 0.09 ^h | 3.50 ± 0.05 ^c | 2.89 ± 0.64 ^f | 15.5 ± 2.15 ^g | |
| | | 60 | 1.07 ± 0.04 ^g | 3.92 ± 0.06 ^a | 3.43 ± 0.19 ^a | 14.5 ± 2.19 ^g | |
| | P_{B} | 45 | 2.50 ± 0.14 ^c | 1.83 ± 0.14 ⁱ | 2.31 ± 0.57 ⁱ | 60.9 ± 3.01 ^a | |
| | | 60 | 3.12 ± 0.18 ^a | 2.00 ± 0.30 ^h | 2.81 ± 0.26 ^f | 64.0 ± 3.25 ^b | |
| | P_{Micro} | 45 | 1.09 ± 0.56 ^g | 2.34 ± 0.39 ^f | 2.62 ± 0.80 ^h | 22.0 ± 1.64 ^e | |
| | | 60 | 1.11 ± 0.62 ^f | 2.72 ± 0.64 ^e | 3.01 ± 0.35 ^d | 19.0 ± 1.25 ^f | |
| | P_{Nano} | 45 | 1.07 ± 0.78 ^g | 3.14 ± 0.25 ^d | 2.65 ± 0.70 ^h | 18.6 ± 1.17 ^f | |
| | | 60 | 1.09 ± 0.92 ^g | 3.59 ± 0.05 ^b | 2.89 ± 0.46 ^d | 17.0 ± 2.15 ^f | |
| | Cambisol | S_{B} | 45 | 2.56 ± 0.13 ^d | 2.35 ± 0.48 ^k | 2.29 ± 0.16 ^g | 56.8 ± 4.52 ^c |
| | | | 60 | 3.17 ± 0.22 ^a | 2.97 ± 0.52 ^h | 2.47 ± 0.35 ^f | 59.8 ± 4.01 ^c |
| | | S_{Micro} | 45 | 1.31 ± 0.59 ⁱ | 3.95 ± 0.56 ^g | 2.80 ± 0.54 ^d | 19.4 ± 1.66 ^e |
| | | | 60 | 1.52 ± 0.73 ^f | 5.53 ± 0.61 ^d | 3.26 ± 0.25 ^a | 17.2 ± 1.64 ^f |
| S_{Nano} | | 45 | 1.14 ± 0.51 ^l | 4.54 ± 0.70 ^e | 2.68 ± 0.48 ^c | 15.4 ± 1.78 ^g | |
| | | 60 | 1.22 ± 0.59 ^j | 5.90 ± 0.52 ^c | 3.14 ± 0.30 ^b | 13.3 ± 2.15 | |
| P_{B} | | 45 | 2.84 ± 0.71 ^b | 2.62 ± 0.12 ^j | 1.73 ± 0.59 ^j | 65.1 ± 3.60 ^a | |
| | | 60 | 3.05 ± 0.71 ^c | 2.83 ± 0.12 ⁱ | 1.97 ± 0.59 ⁱ | 63.8 ± 5.46 ^b | |
| P_{Micro} | | 45 | 1.47 ± 0.04 ^g | 4.37 ± 0.42 ^f | 2.21 ± 0.12 ^h | 21.5 ± 4.12 ^d | |
| | | 60 | 1.82 ± 0.54 ^e | 6.66 ± 0.76 ^b | 2.52 ± 0.50 ^e | 19.7 ± 2.25 ^e | |
| P_{Nano} | | 45 | 1.20 ± 0.76 ^k | 5.54 ± 0.45 ^d | 2.46 ± 0.54 ^f | 15.1 ± 2.14 ^g | |
| | | 60 | 1.41 ± 0.74 ^h | 7.10 ± 0.25 ^a | 2.78 ± 0.64 ^d | 14.3 ± 2.16 ^h | |

Means followed by SE the same letter(s) within each column is not significantly different among treatments ($p < 0.05$).

$$\text{DPS}_{\text{ox}} = [P_{\text{ox}} / (\text{Al}_{\text{ox}} + \text{Fe}_{\text{ox}})] \times 100.$$

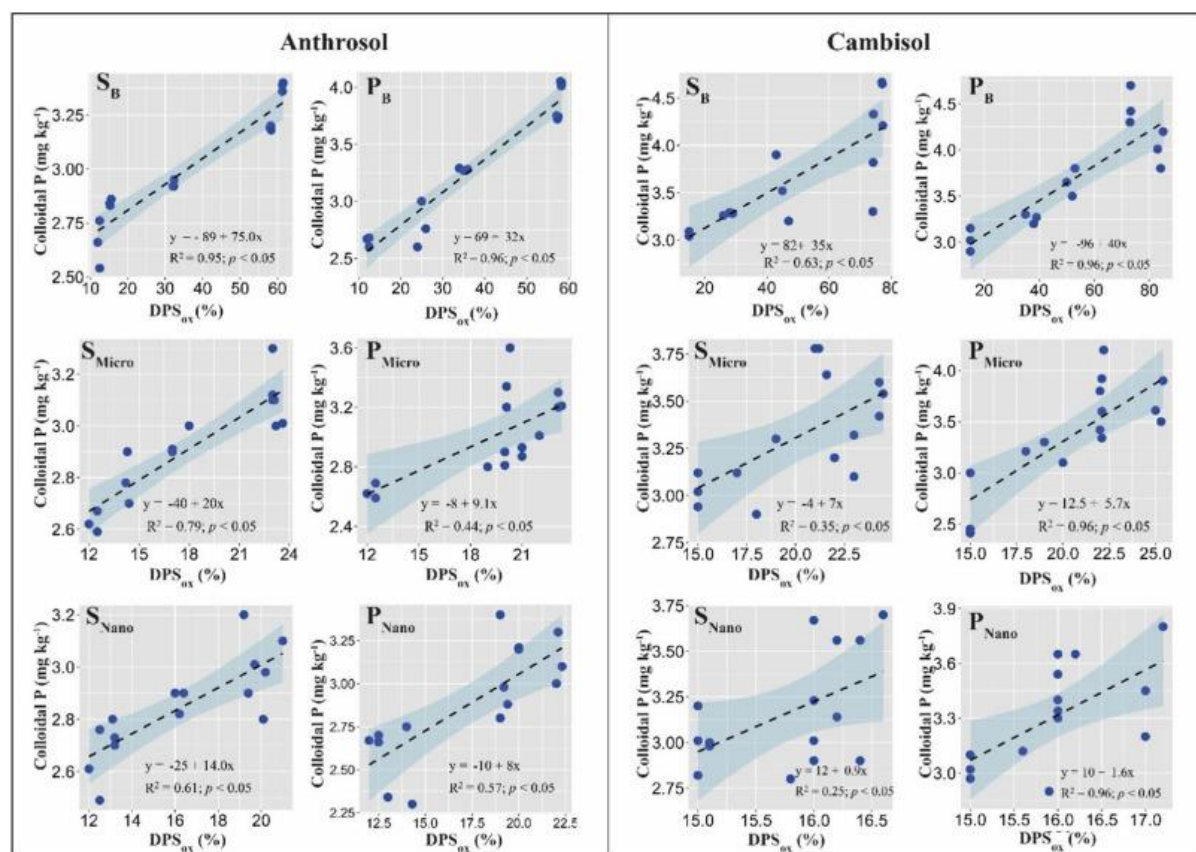
4. Discussion

4.1. Nano and micro manure characterization

The presence of increased ash concentrations in the micro and nano sheep and poultry manures was due to the chemical fractionation that accompanied the size fractionation, and led to the high Fe and Al concentrations (Cao and Harris, 2010), due to the accumulation of inorganic salts in feedstock (Song et al., 2019). The low contents of P in micro and nano manures may be due to the precipitation of P with the Ca or adsorb to the amorphous Fe and Al oxides reduced the P concentration (Hunger et al., 2004). The XRD data proved that the S_{Micro} , S_{Nano} , and P_{Micro} , P_{Nano} had more minerals than S_{B} and P_{B} (Fig. 2). The new peaks in S_{Micro} , P_{Micro} , S_{Nano} , and P_{Micro} showed the presence of gypsum (15°) and struvite (35°), which may act as a slow-release fertilizer, and reduced the colloidal P release. Our results agree with Cooperband and Good (2002), who also observed phosphate minerals in different size fractions of manure (53–0.45 μm). There is also the possibility that some soil contaminated the manure during handling, e.g., some soil be scraped up with the poultry manure, and sheep eat some soil while grazing (Song et al., 2019; Cooperband and Good, 2002).

4.2. Effect of nano and micro manure on colloidal P release

The linear regression analysis and Pearson correlation between DPS and colloidal P (Fig. 5 and Table 3) showed that higher colloidal P in sheep and poultry bulk manures were linked with the higher DPS and low Q_{max} (Table 2) in Anthrosol and Cambisol while low colloidal P concentrations were associated with the low DPS and higher Q_{max} . The high P saturation in soil, triggered the soil colloids dispersion due to high P concentration which released more colloidal P (Siemens et al., 2004). Soils that had DPS_{ox} values >25 and, had greater potential to lose P (Abdala et al., 2015). The Anthrosol and Cambisol incubated with the S_{B} and P_{B} had DPS_{ox} values >25 (Table 2). That is, these two additional indicators showed the susceptibility of the S_{B} and P_{B} treated soils to leak P.



Download : [Download high-res image \(501KB\)](#)

Download : [Download full-size image](#)

Fig. 5. Linear relations between degree of P saturation (DPS_{ox}) (%) and colloidal P (mg kg^{-1}) in Anthrosol and Cambisol incubated with sheep bulk (S_{B}), micro (S_{Micro}), nano (S_{Nano}) and poultry bulk (P_{B}), micro (P_{Micro}) and nano (P_{Nano}) manures.

Table 3. Pearson correlation (R^2) between colloidal P, DPS_{ox} and Q_{max} in sheep and poultry bulk (S_B and P_B), micro (S_{Micro} and P_{Micro}) and nano (S_{Nano} and P_{Nano}) manure amended soils.

| Soil | Manure type and size | Parameters | Colloidal P | DPS_{ox} | Q_{max} |
|-----------|----------------------|-------------|-------------|------------|-----------|
| Anthrosol | S_B | DPS_{ox} | 0.94 | 1.00 | 0.86 |
| | | Q_{max} | 0.94 | 0.86 | 1.00 |
| | | Colloidal P | 1.00 | 0.90 | 0.66 |
| | S_{Micro} | DPS_{ox} | 0.90 | 1.00 | 0.63 |
| | | Q_{max} | 0.66 | 0.63 | 1.00 |
| | | Colloidal P | 1.00 | 0.80 | 0.84 |
| | S_{Nano} | DPS_{ox} | 0.80 | 1.00 | 0.95 |
| | | Q_{max} | 0.84 | 0.95 | 1.00 |
| | | Colloidal P | 1.00 | 0.97 | 0.97 |
| | P_B | DPS_{ox} | 0.97 | 1.00 | 0.94 |
| | | Q_{max} | 0.97 | 0.94 | 1.00 |
| | | Colloidal P | 1.00 | 0.70 | 0.91 |
| | P_{Micro} | DPS_{ox} | 0.70 | 1.00 | 0.95 |
| | | Q_{max} | 0.91 | 0.51 | 1.00 |
| | | Colloidal P | 1.00 | 0.78 | 0.87 |
| | P_{Nano} | DPS_{ox} | 0.78 | 1.00 | 0.89 |
| | | Q_{max} | 0.87 | 0.89 | 1.00 |
| | | Colloidal P | 1.00 | 0.95 | 0.94 |
| Cambisol | S_B | Colloidal P | 1.00 | 0.95 | 0.94 |
| | | DPS_{ox} | 0.95 | 1.00 | 0.86 |
| | | Q_{max} | 0.94 | 0.86 | 1.00 |
| | S_{Micro} | Colloidal P | 1.00 | 0.90 | 0.66 |
| | | DPS_{ox} | 0.90 | 1.00 | 0.63 |
| | | Q_{max} | 0.66 | 0.63 | 1.00 |
| | S_{Nano} | Colloidal P | 0.65 | 0.84 | 0.80 |
| | | DPS_{ox} | 0.75 | 1.00 | 0.91 |
| | | Q_{max} | 0.85 | 0.96 | 1.00 |
| | P_B | Colloidal P | 1.00 | 0.97 | 0.91 |
| | | DPS_{ox} | 0.97 | 1.00 | 0.84 |
| | | Q_{max} | 0.97 | 0.94 | 1.00 |
| | P_{Micro} | Colloidal P | 1.00 | 0.70 | 0.91 |
| | | DPS_{ox} | 0.70 | 1.00 | 0.51 |
| | | Q_{max} | 0.91 | 0.51 | 1.00 |
| | P_{Nano} | Colloidal P | 1.00 | 0.78 | 0.78 |
| | | DPS_{ox} | 0.78 | 1.00 | 0.89 |
| | | Q_{max} | 0.78 | 0.89 | 1.00 |

The high organic matter can blocked the micropores in mineral surfaces and the restriction of P diffusion into them (Hesterberg, 2010), which lower down the Q_{\max} , as shown in S_B and P_B amended soils. However, S_B and P_B also had relatively low binding energy coefficients (Table S5), high DPS (Table 2), and low concentration of Fe_{ox} and Al_{ox} , relative to the nano and micro manures (sheep and poultry). Oxalate selectively extracts hydrous mineral oxides with high P-binding affinity (Liu et al., 2018), and there was a strong correlation between the concentration of ($Fe_{ox} + Al_{ox}$) and Q_{\max} in both soils (Fig. S5). Consequently, we suggested that differences in the concentrations of hydrous oxides of Fe and Al are the principal cause of the effect of particle size on P behavior in our study. Nonetheless, we cannot exclude the possibility that the increased concentrations of calcium carbonate in the nano and micro manures (Fig. 2) may also has contributed (Wang and Li, 2010) in high Q_{\max} in nano and micro manures amended soils. In addition, the OM-Fe/Al complex also carried the colloidal P, which accelerate the release of colloidal P in agriculture soils (Niyungeko et al., 2018), or in fine or nano colloidal fractions, the colloidal P was bound by Fe/Al-organic complexes (Jiang et al., 2015) or else Ca-organic complexes (Li et al., 2021). This is because of a strong association between colloidal minerals (Ca, Fe, Al) and TOC_{coll} (Table S3 and S4). However, the behavior of nano-sized manures needs further investigation. The less release of colloidal P attributed to the struvite and gypsum minerals present in the small size of manures as discussed earlier.

5. Conclusions

The results supported the hypothesis that nano and micro manures decreased the DPS and colloidal P release in both soils. Wet fractionation method produced micro and nano fractions of manure that were enriched in, ash, and minerals (struvite, gypsum, Ca, Al, Fe and Mg phosphate). That is, the effects of size and composition were confounded. Nonetheless, the concentrations of Fe_{ox} and Al_{ox} , ash, and minerals in the different manure size fractions were strongly correlated with increased P-sorption and decreased desorption in both soil types, and with the release of colloidal P, Fe, Al, and Ca. Therefore, we infer that the differences in mineral content between the size fractions dominated the effects of micro and nano manure on colloidal P release. The long-term effect of nano and micro manure on colloidal P and associated soil chemical changes should be investigated.

CRedit authorship contribution statement

Sangar Khan: Conceptualization, Methodology, Software, Validation, Formal analysis, Investigation, Data curation, Writing – original draft, Visualization. **Chunlong Liu:** Writing – review & editing. **Paul J. Milham:** Writing – review & editing. **Kamel Mohamed Eltohamy:** Writing – review & editing. **Yasir Hamid:** Resources. **Junwei Jin:** Writing – review & editing. **Miaomiao He:** Writing – review & editing. **Xinqiang Liang:** Conceptualization, Supervision, Project administration, Funding acquisition.

Declaration of competing interest

The authors declare that they have no known competing financial interests or personal relationships that could have appeared to influence the work reported in this paper.

Acknowledgment

We are grateful for grants from the National Natural Science Foundation of China (22076163), Bingtuan Science and Technology Program (2021DB019), and the Natural Science Foundation of Zhejiang Province (LY18d010007).

Appendix A. Supplementary data

 [Download : Download Word document \(4MB\)](#)

Supplementary material

[Recommended articles](#)

References

Abdala et al., 2015 D.B. Abdala, I.R. da Silva, L. Vergütz, D.L. Sparks

Long-term manure application effects on phosphorus speciation, kinetics and distribution in highly weathered agricultural soils

Chemosphere, 119 (2015), pp. 504-514, [10.1016/j.chemosphere.2014.07.029](https://doi.org/10.1016/j.chemosphere.2014.07.029) ↗

 [View PDF](#) [View article](#) [View in Scopus](#) ↗ [Google Scholar](#) ↗

Brewer et al., 2014 C.E. Brewer, V.J. Chuang, C.A. Masiello, H. Gonnermann, X. Gao, B. Dugan, L.E. Driver, P. Panzacchi, K. Zygourakis, C.A. Davies

New approaches to measuring biochar density and porosity

Biomass Bioenergy, 66 (2014), pp. 176-185, [10.1016/j.biombioe.2014.03.059](https://doi.org/10.1016/j.biombioe.2014.03.059) ↗

 [View PDF](#) [View article](#) [View in Scopus](#) ↗ [Google Scholar](#) ↗

Cao and Harris, 2010 X. Cao, W. Harris

Properties of dairy-manure-derived biochar pertinent to its potential use in remediation

Bioresour. Technol. (2010), [10.1016/j.biortech.2010.02.052](https://doi.org/10.1016/j.biortech.2010.02.052) ↗

[Google Scholar](#) ↗

Chen and Arai, 2020 A. Chen, Y. Arai

Current uncertainties in assessing the colloidal phosphorus loss from soil

Advances in Agronomy (1st ed.), Elsevier Inc. (2020), [10.1016/bs.agron.2020.05.002](https://doi.org/10.1016/bs.agron.2020.05.002) ↗

[Google Scholar](#) ↗

EPA, 2002 U.S. EPA

Arsenic Treatment Technologies for Solid, Waste, and Water

USEPA Rep. EPA-542-R-02-004 (2002)

[Google Scholar](#) ↗

Chen et al., 2018 M. Chen, N. Xu, C. Christodoulatos, D. Wang

Synergistic effects of phosphorus and humic acid on the transport of anatase titanium dioxide nanoparticles in water-saturated porous media

Environ. Pollut., 243 (2018), pp. 1368-1375, [10.1016/j.envpol.2018.09.106](https://doi.org/10.1016/j.envpol.2018.09.106) ↗

 [View PDF](#) [View article](#) [View in Scopus](#) ↗ [Google Scholar](#) ↗

Cooperband and Good, 2002 L.R. Cooperband, L.W. Good

Biogenic phosphate minerals in manure: implications for phosphorus loss to surface waters

Environ. Sci. Technol., 36 (2002), pp. 5075-5082, [10.1021/es025755f](https://doi.org/10.1021/es025755f) ↗

[View in Scopus](#) ↗ [Google Scholar](#) ↗

Dari et al., 2015 B. Dari, V.D. Nair, et al.

Estimation of phosphorus isotherm parameters: a simple and cost-effective procedure

Front. Environ. Sci., 3 (2015)

[Google Scholar](#) ↗

Eduah et al., 2019 J.O. Eduah, E.K. Nartey, M.K. Abekoe, H. Breuning-Madsen, M.N. Andersen

Phosphorus retention and availability in three contrasting soils amended with rice husk and corn cob biochar at varying pyrolysis temperatures

Geoderma, 341 (2019), pp. 10-17, [10.1016/j.geoderma.2019.01.016](https://doi.org/10.1016/j.geoderma.2019.01.016) ↗

 [View PDF](#) [View article](#) [View in Scopus](#) ↗ [Google Scholar](#) ↗

Eltohamy et al., 2021 K.M. Eltohamy, C. Liu, S. Khan, C. Niyungeko, Y. Jin, S.H. Hosseini, F. Li, X. Liang

An internet-based smart irrigation approach for limiting phosphorus release from organic fertilizer-amended paddy soil

J. Clean. Prod., 293 (2021), Article 126254, [10.1016/j.jclepro.2021.126254](https://doi.org/10.1016/j.jclepro.2021.126254) ↗

 [View PDF](#) [View article](#) [View in Scopus](#) [Google Scholar](#)

FAO, 2014 [FAO](#)

World reference base for soil resources 2014

International Soil Classification System for Naming Soils and Creating Legends for Soil Maps, World Soil Resources Reports No. 106 (2014)

[Google Scholar](#)

Fink et al., 2016 [J.R. Fink, A.V. Inda, J. Bavaresco, V. Barrón, J. Torrent, C. Bayer](#)

Adsorption and desorption of phosphorus in subtropical soils as affected by management system and mineralogy

Soil Tillage Res., 155 (2016), pp. 62-68, [10.1016/j.still.2015.07.017](#)

 [View PDF](#) [View article](#) [View in Scopus](#) [Google Scholar](#)

Fresne et al., 2021 [M. Fresne, P. Jordan, O. Fenton, P.E. Mellander, K. Daly](#)

Soil chemical and fertilizer influences on soluble and medium-sized colloidal phosphorus in agricultural soils

Sci. Total Environ., 754 (2021), [10.1016/j.scitotenv.2020.142112](#)

[Google Scholar](#)

Gérard, 2016 [F. Gérard](#)

Clay minerals, iron/aluminum oxides, and their contribution to phosphate sorption in soils – a myth revisited

Geoderma, 262 (2016), pp. 213-226, [10.1016/j.geoderma.2015.08.036](#)

 [View PDF](#) [View article](#) [View in Scopus](#) [Google Scholar](#)

Gottselig et al., 2014 [N. Gottselig, R. Bol, V. Nischwitz, H. Vereecken, W. Amelung, E. Klumpp](#)

Distribution of phosphorus-containing fine colloids and nanoparticles in stream water of a forest catchment

Vadose Zo. J., 13 (2014), [10.2136/vzj2014.01.0005](#)

[Google Scholar](#)

Hesterberg, 2010 [D. Hesterberg](#)

Macroscale chemical properties and X-ray absorption spectroscopy of soil phosphorus

Developments in Soil Science (1st ed.), Elsevier B.V. (2010), [10.1016/s0166-2481\(10\)34011-6](#)

[Google Scholar](#)

Hunger et al., 2004 [S. Hunger, H. Cho, J.T. Sims, D.L. Sparks](#)

Direct speciation of phosphorus in alum-amended poultry litter: solid-state ³¹P NMR investigation

Environ. Sci. Technol., 38 (2004), pp. 674-681, [10.1021/es034755s](#)

[View in Scopus](#) [Google Scholar](#)

Ilg et al., 2008 [K. Ilg, P. Dominik, M. Kaupenjohann, J. Siemens](#)

Phosphorus-induced mobilization of colloids: model systems and soils

Eur. J. Soil Sci., 59 (2008), pp. 233-246, [10.1111/j.1365-2389.2007.00982.x](#)

[View in Scopus](#) [Google Scholar](#)

Jiang et al., 2015 [X. Jiang, R. Bol, S. Willbold, H. Vereecken, E. Klumpp](#)

Speciation and distribution of P associated with Fe and Al oxides in aggregate-sized fraction of an arable soil

Biogeosciences, 12 (2015), pp. 6443-6452, [10.5194/bg-12-6443-2015](#)

[View in Scopus](#) [Google Scholar](#)

Khan et al., 2021 [S. Khan, P.J. Milham, K.M. Eltohamy, Y. Jin, Z. Wang, X. Liang](#)

Phytate exudation by the roots of *Pteris vittata* can dissolve colloidal FePO₄

Environ. Sci. Pollut. Res. (2021), [10.1007/s11356-021-16534-2](https://doi.org/10.1007/s11356-021-16534-2) ↗

[Google Scholar](#) ↗

Khan et al., 2022 S. Khan, P.J. Milham, K. Mohamed, Y. Hamid, F. Li, J. Jin, M. He, X. Liang

***Pteris vittata* plantation decrease colloidal phosphorus contents by reducing degree of phosphorus saturation in manure amended soils**

J. Environ. Manag., 304 (2022), Article 114214, [10.1016/j.jenvman.2021.114214](https://doi.org/10.1016/j.jenvman.2021.114214) ↗

 [View PDF](#) [View article](#) [View in Scopus](#) ↗ [Google Scholar](#) ↗

Li et al., 2021 F. Li, Q. Zhang, E. Klumpp, R. Bol, V. Nischwitz, Z. Ge, X. Liang

Organic carbon linkage with soil colloidal phosphorus at regional and field scales: insights from size fractionation of fine particles

Environ. Sci. Technol., 55 (2021), pp. 5815-5825, [10.1021/acs.est.0c07709](https://doi.org/10.1021/acs.est.0c07709) ↗

[View in Scopus](#) ↗ [Google Scholar](#) ↗

Liang et al., 2016 X. Liang, Y. Jin, et al.

Release and migration of colloidal phosphorus from a typical agricultural field under long-term phosphorus fertilization in southeastern China

J. Soils Sediments, 16 (3) (2016), pp. 842-853

[CrossRef](#) ↗ [View in Scopus](#) ↗ [Google Scholar](#) ↗

Liang et al., 2010 X. Liang, J. Liu, Y. Chen, H. Li, Y. Ye, Z. Nie, M. Su, Z. Xu

Effect of pH on the release of soil colloidal phosphorus

J. Soils Sediments, 10 (2010), pp. 1548-1556, [10.1007/s11368-010-0275-6](https://doi.org/10.1007/s11368-010-0275-6) ↗

[View in Scopus](#) ↗ [Google Scholar](#) ↗

Liu et al., 2018 Y. Liu, Z. Zhu, X. He, C. Yang, Y. Du

Mechanisms of rice straw biochar effects on phosphorus sorption characteristics of acid upland red soils

Chemosphere, 207 (2018), pp. 267-277, [10.1016/j.chemosphere.2018.05.086](https://doi.org/10.1016/j.chemosphere.2018.05.086) ↗

 [View PDF](#) [View article](#) [View in Scopus](#) ↗ [Google Scholar](#) ↗

Makris et al., 2006 K.C. Makris, J.H. Grove, et al.

Colloid-mediated vertical phosphorus transport in a waste-amended soil

Geoderma, 136 (1-2) (2006), pp. 174-183

 [View PDF](#) [View article](#) [View in Scopus](#) ↗ [Google Scholar](#) ↗

McGechan, 2002 M.B. McGechan

Effects of timing of slurry spreading on leaching of soluble and particulate inorganic phosphorus explored using the MACRO model

Biosyst. Eng., 83 (2002), pp. 237-252, [10.1006/bioe.2002.0115](https://doi.org/10.1006/bioe.2002.0115) ↗

 [View PDF](#) [View article](#) [View in Scopus](#) ↗ [Google Scholar](#) ↗

Missong et al., 2016 A. Missong, R. Bol, S. Willbold, J. Siemens, E. Klumpp

Phosphorus forms in forest soil colloids as revealed by liquid-state ³¹P-NMR

J. Plant Nutr. Soil Sci., 179 (2016), pp. 159-167, [10.1002/jpln.201500119](https://doi.org/10.1002/jpln.201500119) ↗

[View in Scopus](#) ↗ [Google Scholar](#) ↗

Moradi et al., 2020 G. Moradi, R. Bol, L. Trbojevic, A. Missong, R. Mörchen, B. Fuentes, S.M. May, E. Lehndorff, E. Klumpp

Contrasting depth distribution of colloid-associated phosphorus in the active and abandoned sections of an alluvial fan in a hyper-arid region of the Atacama Desert

Glob. Planet. Change, 185 (2020), [10.1016/j.gloplacha.2019.103090](https://doi.org/10.1016/j.gloplacha.2019.103090) ↗

[Google Scholar](#) »

Murphy and Riley, 1962 J. Murphy, J.P. Riley

A modified single solution method for the determination of phosphate in natural waters

Anal. Chim. Acta (1962), [10.1016/S0003-2670\(00\)88444-5](https://doi.org/10.1016/S0003-2670(00)88444-5) »

[Google Scholar](#) »

Niyungeko et al., 2018 C. Niyungeko, X. Liang, C. Liu, M. Sheteiwy, H. Zhang, J. Zhou, G. Tian, Liu Z. Wen

Effect of biogas slurry application rate on colloidal phosphorus leaching in paddy soil: a column study

Geoderma, 325 (2018), pp. 117-124, [10.1016/j.geoderma.2018.03.036](https://doi.org/10.1016/j.geoderma.2018.03.036) »

 [View PDF](#) [View article](#) [View in Scopus](#) » [Google Scholar](#) »

Pagel et al., 2008 H. Pagel, K. Ilg, J. Siemens, M. Kaupenjohann

Total phosphorus determination in colloid-containing soil solutions by enhanced persulfate digestion

Soil Sci. Soc. Am. J. (2008), [10.2136/sssaj2007.0178n](https://doi.org/10.2136/sssaj2007.0178n) »

[Google Scholar](#) »

Pan et al., 2019 X. Pan, L. Li, et al.

Distribution characteristics and pollution risk evaluation of the nitrogen and phosphorus species in the sediments of Lake Erhai, Southwest China

Environ. Sci. Pollut. Res., 26 (22) (2019), pp. 22295-22304, [10.1007/s11356-019-05489-0](https://doi.org/10.1007/s11356-019-05489-0) »

[View in Scopus](#) » [Google Scholar](#) »

Schmieder et al., 2018 F. Schmieder, L. Bergström, M. Riddle, J.P. Gustafsson, W. Klysubun, F. Zehetner, L. Condrón, H. Kirchmann

Phosphorus speciation in a long-term manure-amended soil profile – evidence from wet chemical extraction, 31P-NMR and P K-edge XANES spectroscopy

Geoderma, 322 (2018), pp. 19-27, [10.1016/j.geoderma.2018.01.026](https://doi.org/10.1016/j.geoderma.2018.01.026) »

 [View PDF](#) [View article](#) [View in Scopus](#) » [Google Scholar](#) »

Schwartz et al., 2011 R.C. Schwartz, T.H. Dao, J.M. Bell

Manure and mineral fertilizer effects on seasonal dynamics of bioactive soil phosphorus fractions

Agron. J., 103 (2011), pp. 1724-1733, [10.2134/agronj2011.0165](https://doi.org/10.2134/agronj2011.0165) »

[View in Scopus](#) » [Google Scholar](#) »

Sharma et al., 2017 R. Sharma, R.W. Bella, et al.

Dissolved reactive phosphorus played a limited role in phosphorus transport via runoff, throughflow and leaching on contrasting cropping soils from southwest Australia

Sci. Total Environ. (2017)

[Google Scholar](#) »

Siemens et al., 2004 J. Siemens, K. Ilg, F. Lang, M. Kaupenjohann

Adsorption controls mobilization of colloids and leaching of dissolved phosphorus

Eur. J. Soil Sci., 55 (2004), pp. 253-263, [10.1046/j.1365-2389.2004.00596.x](https://doi.org/10.1046/j.1365-2389.2004.00596.x) »

[View in Scopus](#) » [Google Scholar](#) »

Song et al., 2019 B. Song, M. Chen, L. Zhao, H. Qiu, X. Cao

Physicochemical property and colloidal stability of micron- and nano-particle biochar derived from a variety of feedstock sources

Sci. Total Environ., 661 (2019), pp. 685-695, [10.1016/j.scitotenv.2019.01.193](https://doi.org/10.1016/j.scitotenv.2019.01.193) »

 [View PDF](#) [View article](#) [View in Scopus](#) » [Google Scholar](#) »

Wang et al., 2021 Z. Wang, L. Chen, et al.

Reduced colloidal phosphorus loss potential and enhanced phosphorus availability by manure-derived biochar addition to paddy soils

Geoderma, 402 (2021), p. 115348, [10.1016/j.geoderma.2021.115348](https://doi.org/10.1016/j.geoderma.2021.115348) >

 [View PDF](#) [View article](#) [View in Scopus >](#) [Google Scholar >](#)

Wang and Li, 2010 Q. Wang, Y. Li

Phosphorus adsorption and desorption behavior on sediments of different origins

J. Soils Sediments, 10 (2010), pp. 1159-1173, [10.1007/s11368-010-0211-9](https://doi.org/10.1007/s11368-010-0211-9) >

[View in Scopus >](#) [Google Scholar >](#)

Wang et al., 2013 D. Wang, W. Zhang, X. Hao, D. Zhou

Transport of biochar particles in saturated granular media: effects of pyrolysis temperature and particle size

Environ. Sci. Technol., 47 (2013), pp. 821-828, [10.1021/es303794d](https://doi.org/10.1021/es303794d) >

[View in Scopus >](#) [Google Scholar >](#)

Xiao et al., 2020 Y. Xiao, J. Puig-Bargués, B. Zhou, Q. Li, Y. Li

Increasing phosphorus availability by reducing clogging in drip fertigation systems

J. Clean. Prod., 262 (2020), [10.1016/j.jclepro.2020.121319](https://doi.org/10.1016/j.jclepro.2020.121319) >

[Google Scholar >](#)

Yang et al., 2019 W. Yang, J. Shang, P. Sharma, B. Li, K. Liu, M. Flury

Colloidal stability and aggregation kinetics of biochar colloids: effects of pyrolysis temperature, cation type, and humic acid concentrations

Sci. Total Environ., 658 (2019), pp. 1306-1315, [10.1016/j.scitotenv.2018.12.269](https://doi.org/10.1016/j.scitotenv.2018.12.269) >

 [View PDF](#) [View article](#) [View in Scopus >](#) [Google Scholar >](#)

Zang et al., 2013 L. Zang, G.M. Tian, X.Q. Liang, M.M. He, Q.B. Bao, J.H. Yao

Profile distributions of dissolved and colloidal phosphorus as affected by degree of phosphorus saturation in paddy soil

Pedosphere (2013), [10.1016/S1002-0160\(12\)60088-5](https://doi.org/10.1016/S1002-0160(12)60088-5) >

[Google Scholar >](#)

Zhang et al., 2013 H. Zhang, Y. Luo, T. Makino, L. Wu, M. Nanzyo

The heavy metal partition in size-fractions of the fine particles in agricultural soils contaminated by waste water and smelter dust

J. Hazard. Mater., 248-249 (2013), pp. 303-312, [10.1016/j.jhazmat.2013.01.019](https://doi.org/10.1016/j.jhazmat.2013.01.019) >

 [View PDF](#) [View article](#) [View in Scopus >](#) [Google Scholar >](#)

Cited by (4)

Improved phosphorus availability and reduced degree of phosphorus saturation by biochar-blended organic fertilizer addition to agricultural field soils

2023, Chemosphere

[Show abstract](#) 

Nano and fine colloids suspended in the soil solution regulate phosphorus desorption and lability in organic fertiliser-amended soils

2023, Science of the Total Environment

[Show abstract](#) 



Copyright © 2023 Elsevier B.V. or its licensors or contributors.
ScienceDirect® is a registered trademark of Elsevier B.V.



2022, Water (Switzerland)

[View Abstract](#)

© 2022 Elsevier B.V. All rights reserved.